JCTC Journal of Chemical Theory and Computation

pubs.acs.org/JCTC Article

# Combination of a Voronoi-Type Complex Absorbing Potential with the XMS-CASPT2 Method and Pilot Applications

Quan Manh Phung, Yuki Komori, Takeshi Yanai,* Thomas Sommerfeld,* and Masahiro Ehara*

Cite This: J. Chem. Theory Comput. 2020, 16, 2606−2616 Read Online

ACCESS | Metrics & More | Article Recommendations | Supporting Information

**ABSTRACT:** Electronic resonances are metastable $(N + 1)$ electron states, in other words, discrete states embedded in an electronic continuum. While great progress has been made for certain types of resonances—for example, temporary anions created by attaching one excess electron to a closed shell neutral—resonances in general remain a great challenge of quantum chemistry because a successful description of the decay requires a balanced description of the bound and continuum aspect of the resonance. Here, a smoothed Voronoi complex absorbing potential (CAP) is combined with the XMS-CASPT2 method, which enables us to address the balance challenge by appropriate choice of the CAS space. To reduce the computational cost, the method is implemented in the projected scheme. In this pilot application, three temporary anions serve as benchmarks: the $\pi^*$ resonance state of formaldehyde; the $\pi^*$ and $\sigma^*$ resonance states of chloroethene as functions of the C−Cl bond dissociation coordinate; and the $^4\Pi_u$ and $^2\Pi_u$ resonance states of $N_2^-$. The convergence of the CAP/XMS-CASPT2 results has been systematically examined with respect to the size of the active space. Resonance parameters predicted by the CAP/XMS-CASPT2 method agree well with CAP/SAC-CI results (deviations of about 0.15 eV); however, as expected, CAP/XMS-CASPT2 has clear advantages in the bond dissociation region. The advantages of CAP/XMS-CASPT2 are further demonstrated in the calculations of $^4\Pi_u$ and $^2\Pi_u$ resonance states of $N_2^-$ including their $^3\Sigma_u^+$ and $^3\Delta_u$ parent states. Three of the involved states ($^2\Pi_u$, $^3\Sigma_u^+$, and $^3\Delta_u$) possess multireference character, and CAP/XMS-CASPT2 can easily describe these states with a relatively modest active space.

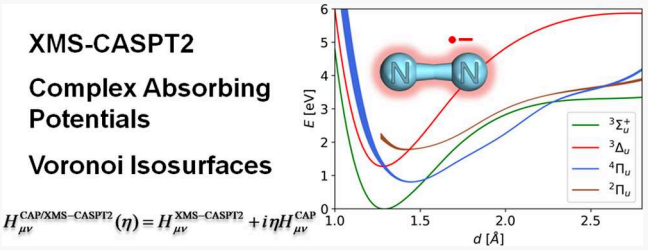




## INTRODUCTION

Resonance states or resonances are metastable states with at least one open decay channel. Typical examples for electronic resonances are temporary anions,[1] multiply-charged anions,[2] core-hole states decaying by Auger processes,[3] and electronic relaxation of valence-ionized clusters.[4] Owing to their excess energy, electronic resonances play often the role of reactive intermediates in electron-induced or electron-catalyzed processes.[5,6]

Resonance states of $(N + 1)$ electron systems are characterized by their energy, $E_r$, above the $N$-electron system and by their width, $\Gamma$, which is inversely related to their lifetime, $\tau = \hbar/\Gamma$.

Because resonances are part of the continuum, they cannot be represented by square-integrable ($L^2$) wavefunctions in a straightforward way. Instead, computational methods for resonances need to take the continuum nature of a decaying state either explicitly (scattering methods) or implicitly ($L^2$-methods) into account. However, at the same time, electronic resonances represent a many-electron system, and especially the decay rates are highly sensitive to a balanced treatment of electron correlation in the $N$ and $(N + 1)$ electron states. This challenge is often referred to as the continuum-correlation problem.

As is so often the case, no ideal solution exists. Regarding the continuum aspect, scattering methods explicitly deal with the continuum nature of the wavefunction and compute the electron cross section, from which $E_r$ and $\Gamma$ can be extracted by numerical analysis. In contrast, $L^2$-methods transform the continuum problem so that only square-integrable wavefunctions are used, and $E_r$ and $\Gamma$ are found by analyzing the behavior of the eigenvalues of a parametrized Hamiltonian. Although computing the scattering cross section in the framework of $L^2$-methods is usually anything but trivial, $L^2$-methods have clear advantages regarding the ease of combination with high-level many-body methods.

Electron correlation is vital for computing reliable electron affinities, in general, and for resonances it is even more important. When computing electron affinities of bound anions, electron-correlation needs to describe the $N$ and the $(N + 1)$-electron systems in a balanced way. Methods that

Received: October 15, 2019
Published: February 27, 2020





https://dx.doi.org/10.1021/acs.jctc.9b01032
J. Chem. Theory Comput. 2020, 16, 2606−2616

guarantee this balance are called size-extensive (note: not size-intensive). In resonances, in addition, the wavefunction for the $(N + 1)$ system combines aspects of the discrete state, which has $(N + 1)$-electron character, with continuum aspects, which has $N$-electron character because one electron occupies a diffuse pseudo-continuum orbital, in other words, resonance wavefunctions need to be internally size-extensive, too.

How well a given method fulfills the above requirements for a given resonance can be tested at threshold. The resonance position, $E_r$, is determined by the inherent size-extensity of the method, the width, $\Gamma$, however, is determined by the internal size-extensity of the method. Clearly, $\Gamma$ must vanish where $E_r = 0$ and the resonance is turned into a bound state.

In this paper, the focus is on the complex absorbing potential (CAP) method,[7,8] which is a standard $L^2$-method. Other examples for $L^2$-methods include the complex scaling method,[9] stabilization method,[10] and analytical continuation of the coupling constant (ACCC) method.[11−13] In all $L^2$-methods, the resonance parameters, $E_r$ and $\Gamma$, are found by analyzing the eigenvalues of a parametrized Hamiltonian. Thus, a "single-point calculation" of a single $E_r$ and $\Gamma$ pair involves the computation of several eigenvalues for several values of the parameter, and in general, multistate electronic structure methods are needed, such as configuration interaction-type methods, Green's function approaches, or equation-of-motion type approaches. The exception is the ACCC method, which requires only the ground state (GS), however, owing to the extrapolation step, ACCC is limited to "close-to-threshold" resonances.

CAPs served originally as tools in wave packet propagation to avoid reflections at the boundary of the numerical grid, and their use for computing resonance states was discovered only later (see ref 8 and references therein). In electronic structure theory, CAPs were initially combined with multireference configuration-interaction theory,[14−18] Green's function methods,[19,20] and coupled-cluster related orbital theory.[21] More recently, the interest shifted to methods based on symmetry-adapted cluster-configuration interaction (SAC-CI) method[22] and equation-of-motion coupled cluster (EOM-CC) methods,[23−25] which are closely related. Both methods yield by construction multiple states (MS) and fulfill the balance requirements as long as the decaying state and the continuum states belong to the same excitation class, for example, for temporary anions the resonance and the continuum are represented by one-particle states. However, both methods require a single-configuration reference state from which the excitation space can be built and will become impractical in bond breaking situations or in the study of Feshbach resonances.

The most recent developments address this need: CAPs were combined with the extended multiconfiguration quasi-degenerate second-order perturbation theory (XMCQDPT2) method[26] to investigate Feshbach resonances. We note that CAPs were very recently also combined with the XMS-CASPT2 method;[27] however, the primary focus of ref 27 is the visualization of complex orbitals, while the theoretical method for creating these orbitals is secondary and issues such as performance and accuracy were not considered.

Multireference approaches represent the most natural way to describe electronic states in the bond dissociation region or states with several excited electrons.[28−30] Static correlation is dealt with in an initial complete active space self-consistent field (CASSCF) step, and a state-averaged (SA) CASSCF treatment can be used to obtain the references of a GS and several low-lying excited states. Dynamic correlation is then treated in a second step, and the most popular model is probably complete-active-space second-order perturbation theory (CASPT2).[31,32] Extensions to MS are MS-CASPT2[33] and its generalization with Granovsky's extension[34] (XMS-CASPT2)[35] as well as MCQDPT2[36,37] and XMCQDPT2.[34] The main difference between (X)MS-CASPT2 and (X)MCQDPT2 lies in the formalism of the expansion of the first-order wave function; (X)MS-CASPT2 is based on an internally contracted basis ansatz, whereas the (X)MCQDPT2 uses an uncontracted determinant basis for the expansion. Note that the compactness of an internally contracted basis in (X)MS-CASPT2 has been exploited to combine it with the density matrix renormalization group wave function formalism.[38]

Turning to the CAP itself, we note that in the recent CAP/XMCQDPT2[26] and CAP/XMS-CASPT2[27] combinations, so-called Cartesian and spherical box-CAPs were employed. In a box-CAP, the CAP vanishes in a central region, is switched on at a particular cutoff radius, and then grows in some manner—typically quadratically—after that. The difference between a Cartesian and a spherical box-CAP is whether the potential is defined for each Cartesian or for a radial coordinate. Here, we combine XMS-CASPT2 with a smooth Voronoi CAP,[39,40] which is similar to a box-CAP that is zero in the inner region and possesses a cutoff radius, however, the switching coordinate is the distance-to-the-nearest-atom. Thus, isocontour surfaces of a Voronoi CAP resemble smoothed van-der-Waals surfaces of the molecular system.

For small compact molecules, Voronoi CAPs offer no great advantages over box-CAPs, indeed, the need to compute the Voronoi matrix elements numerically represents a major disadvantage in these cases. However, Voronoi CAPs show the same symmetry as the Hamiltonian and, more importantly, adapt to changes in molecular geometry far more flexibly than box-CAPs.[40−42] As an extreme example, consider the following solvation model: a temporary anion in the coordinate origin surrounded by six solvent molecules at a distance $R$ from the origin centered on the positive and negative Cartesian axes. If $R$ is increased from a small value representing solvation to a large value representing the unsolvated molecule, the cutoff parameter of a box-CAP needs to be increased accordingly so as to include the solvent molecules in the CAP-box, and converging the basis set will become increasingly difficult if not impossible. In contrast, a Voronoi CAP will adapt to any change in $R$ without change of its cutoff parameter, and the one-particle basis set needed to converge the CAP calculation will be largely independent of $R$. As stated above, this example is somewhat artificial; however, it clearly demonstrates that Voronoi CAPs represent a more natural choice in bond-breaking or cluster dissociation situations.

Here, we present a combination of a Voronoi CAP with the XMS-CASPT2 method. Similar to CAP/CI,[18] CAP/SAC-CI,[22] and CAP/XMCQDPT2,[26] the CAP calculation itself is performed in the projected scheme, that is, first a suitable number of eigenstates of the real Hamiltonian—typically all states up to a certain energy—are computed, and then the CAP Hamiltonian is projected into this subspace of the real Hamiltonian. The method has been implemented in the orz program package.[43] As a first pilot application, we choose two cases that enable us to directly compare CAP/XMS-CASPT2 with CAP/SAC-CI: the well-characterized resonance state of


https://dx.doi.org/10.1021/acs.jctc.9b01032
J. Chem. Theory Comput. 2020, 16, 2606−2616

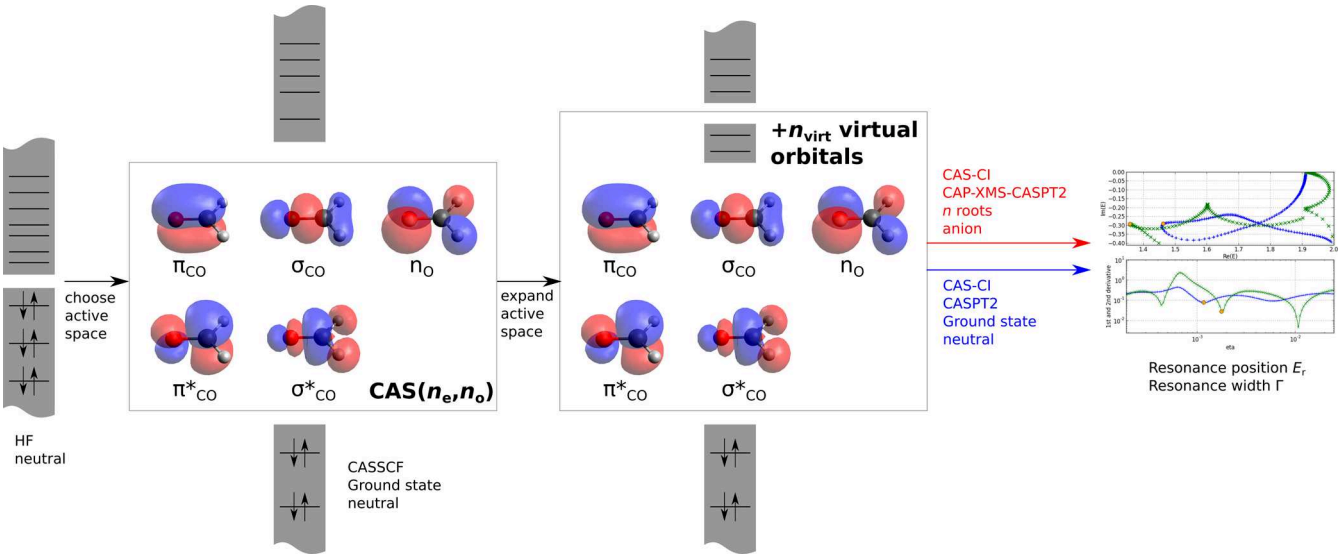


**Figure 1.** Schematic representation of the calculations performed in this work. CAS($n_e$,$n_o$) and $n_{virt}$, which determine the size of the active space, can be simultaneously varied.

formaldehyde and the potential energy curves (PECs) of the $\sigma^*$ and $\pi^*$ resonances of chloroethene along the C−Cl dissociation coordinate. Extension of the active space and the orbitals included in the XMS-CASPT2 calculations are systematically examined. As an example for resonances with multireference character, we compare the $^4\Pi_u$ and $^2\Pi_u$ resonance states of $N_2^-$.

## METHOD

**Theory.** A CAP calculation yields the complex Siegert energy of a resonance as[44,45]

$$E_{res} = E_r - i\Gamma/2 \tag{1}$$

where $E_r$ and $\Gamma$, are the resonance position and width. To do so, a CAP, $-iW$, is added to the physical Hamiltonian, $H$, yielding a non-Hermitian, complex-symmetric Hamiltonian

$$H(\eta) = H - i\eta W \tag{2}$$

where $\eta$ is a strength parameter. In this work, we use a smooth Voronoi CAP which wraps around the molecule like a van der Waals cavity.[39] In principle, the resonance energy, $E_{res}$, is independent of $\eta$ provided $\eta > 0$; however, if finite basis sets are used, $E_{res}$ becomes $\eta$-dependent and is obtained from one of the $\eta$-trajectories of the eigenvalues of $H(\eta)$. The eigenvalue representing the resonance can normally be identified by its "stabilization", in other words, its $\eta$-velocity shows a minimum, and it is at this CAP strength at which the resonance energy should be evaluated.[8,19] Moreover, a first-order correction for CAP artifacts can be applied, and the corrected trajectories, $E(\eta) - dE(\eta)/d(\ln \eta)$, were computed similar to previous studies.[8,22,41]

In this study, we evaluate the matrix elements of $H(\eta)$ as follows

$$H_{\mu\nu}^{CAP/XMS\text{-}CASPT2}(\eta) = H_{\mu\nu}^{XMS\text{-}CASPT2} - i\eta H_{\mu\nu}^{CAP} \tag{3}$$

using the effective Hamiltonian matrix determined by usual (X)MS-CASPT2 calculations, denoted $H_{\mu\nu}^{XMS\text{-}CASPT2}$. Equation 3 is thus represented in the model space spanned by the same state basis as used for forming $H_{\mu\nu}^{XMS\text{-}CASPT2}$, given as[33,35]

$$H_{\mu\nu}^{XMS\text{-}CASPT2} = H_{\mu\nu}^{ref} + \frac{1}{2}(H_{\mu\nu}^{(2)} + H_{\nu\mu}^{(2)}) \tag{4}$$

where $H_{\mu\nu}^{ref}$ are the matrix elements of XMS-rotated CASSCF energies written as $H_{\mu\nu}^{ref} = \langle\mu|H|\nu\rangle$ and $H_{\mu\nu}^{(2)}$ are XMS-CASPT2 second-order energy corrections given by $H_{\mu\nu}^{(2)} = \langle\mu|H|\Psi_\nu^{(1)}\rangle$. Note that $|\mu\rangle$ and $|\nu\rangle$ denote XMS-rotated CASSCF wave functions. In principle, the CAP part of eq 3 should be evaluated at the CASPT2 level for consistency; however, as has been shown in ref 26 for the uncontracted CAP/XMCQDPT2 variant, it is sufficient—and computationally less costly—to evaluate the CAP matrix elements in an approximate manner using the CASSCF wave functions

$$H_{\mu\nu}^{CAP} = \langle\mu|W|\nu\rangle \tag{5}$$

because these expressions can be readily evaluated using the one-electron reduced density matrix and transition density matrix of XMS-rotated CASSCF wave functions. The XMS-CASPT2 matrix (eq 4) and $\eta$-independent CAP matrix (eq 5) may be separately calculated and stored prior to the $\eta$-trajectory calculations.

**Computational Details.** Using CAP/SAC-CI and CAP/XMS-CASPT2, we study the $\pi^*$ resonance of $H_2CO^-$ ($^2B_1$ state), the $\sigma^*$ and $\pi^*$ resonances of $CH_2CHCl^-$ ($^2A'$ and $^2A''$ states, respectively), as well as the $^4\Pi_u$ and $^2\Pi_u$ resonances of $N_2^-$. All optimized geometries in this work were obtained at the B3LYP/cc-pVDZ level of theory.[46,47] Cartesian coordinates can be found in the Supporting Information.

All CAP/XMS-CASPT2 calculations were performed following the procedure described in Figure 1. First, the neutral molecule was calculated at the Hartree−Fock (HF) level. A set of $n_o$ strongly correlated orbitals, which are suitable for describing static correlation, was selected and included in an active space, denoted as CAS($n_e$,$n_o$). This active space was optimized in a subsequent CASSCF calculation of the GS of the neutral molecule. In the next step, the active space was augmented with a set of $n_{virt}$ lowest (in energy) virtual (or diffuse) orbitals, which are eigenfunctions of the generalized Fock operator built from the CAS($n_e$,$n_o$) density matrix. We note that this way of choosing virtual orbitals may not be fully optimized; however, it allows us to systematically investigate


https://dx.doi.org/10.1021/acs.jctc.9b01032
J. Chem. Theory Comput. 2020, 16, 2606−2616

the convergence of the results with respect to $n_{virt}$. The GS of the neutral molecule was calculated with CASCI/CASPT2 using this active space CAS($n_e$,$n_o$ + $n_{virt}$) ($n_o$ + $n_{virt}$ orbitals containing $n_e$ electrons). On the other hand, $n_{virt}$ states of the anion were calculated with CASCI/SA-XMS-CASPT2 using the same set of orbitals and the same orbital space ($n_o$ + $n_{virt}$ active orbitals). For convenience of description, we use a unified notation CAS($n_e$,$n_o$) + $n_{virt}$ to represent the CAS($n_e$,$n_o$ + $n_{virt}$) and CAS($n_e$ + 1,$n_o$ + $n_{virt}$) active spaces of the neutral molecule and the anion, respectively. The resonance position $E_r$ and width Γ were then extracted by analyzing the $\eta$-trajectories.

Both $E_r$ and Γ depend on various factors, such as the character of the active orbitals,[26] the one particle basis set, and the CAP cutoff.[22] The latter two have been extensively examined in a series of studies using CAP/SAC-CI.[22,40,41,48] In this work, we focus on the impact of the first factor by using different combinations of CAS($n_e$,$n_o$) and $n_{virt}$. We study the $^2B_1$ resonance of $H_2CO^-$, employing four CAS($n_e$,$n_o$) active spaces. The largest one is CAS(6,5) comprising one ($\sigma_{CO}$, $\sigma^*_{CO}$) pair, one ($\pi_{CO}$, $\pi^*_{CO}$) pair, and one oxygen lone pair (see also Figure 1). This active space is expected to give a good description of the wave function for the subsequent PT2 treatment.[49] The active space can be reduced by removing the ($\sigma_{CO}$, $\sigma^*_{CO}$) pair, giving a CAS(4,3); and the oxygen lone pair, leading to a CAS(2,2). Finally, one can employ the smallest "active space" CAS(0,0), that is, the CASSCF calculation was skipped and the HF canonical orbitals were used instead. For each CAS($n_e$,$n_o$), we used a wide range of $n_{virt}$ from 5 to 17 orbitals. All virtual orbitals included in this way always correspond to the $n_{virt}$ lowest virtual orbitals in $b_1$ symmetry.

Notice that in the calculations with CAS(0,0) + $n_{virt}$, the GS of the neutral molecule was calculated with a CAS(0,0 + $n_{virt}$) "active space", that is, HF. Consequently, CASPT2 calculations on top of this active space give results which are (i) independent of the $n_{virt}$ value and (ii) similar to those of standard MP2. We note that owing to a modified zeroth-order Hamiltonian, CAS(0,0 + $n_{virt}$)-PT2 and MP2 results do not strictly coincide (normally, ionization-potential-electron-affinity (IPEA) and imaginary shifts are employed in CASPT2; if these are set to 0, the two methods are equivalent).

To study the $\sigma^*$ and $\pi^*$ resonances of $CH_2CHCl^-$, we used two CAS($n_e$,$n_o$) active spaces: CAS(0,0) (or HF) and CAS(2,2). The latter active space consists of the ($\sigma_{CCl}$, $\sigma^*_{CCl}$) pair (see Figure S1) which describes the C−Cl bond dissociation. The active spaces were then expanded by adding $n_{virt}$ = 17 $a'$ or 10 $a''$ virtual orbitals, respectively.

In the applications to the $^4\Pi_u$ and $^2\Pi_u$ resonance states of $N_2^-$, we employed a minimal active space comprising all nitrogen 2p orbitals (6 active orbitals in total). In all calculations, $D_{2h}$ point group symmetry was exploited and the cc-pVTZ + [2s5p2d] basis set was employed. We used $n_{virt}$ = 10, including five $\pi_{ux}$ ($b_{3u}$) and five $\pi_{uy}$ ($b_{2u}$) virtual orbitals to maintain the symmetry of the wave function.

For the CAP/SAC-CI calculations, the SAC-CI SD-$R$ method[50,51] employing the direct algorithm for the calculating $\sigma$-vectors[52] was used for the electron-attachment (EA) scheme. Nonvariational calculations denoted as SAC-CI NV were adopted. To reduce the computational cost, we employed the perturbation selection for both $R$ and $S$ operators.[53] Following the benchmark calculations regarding the energy thresholds of operator selection,[54] we adopted so-called Level Four accuracy with energy thresholds of $\lambda_g = 5 \times 10^{-6}$ and $\lambda_e = 5 \times 10^{-7}$ Hartree in the present calculations.

For the CAP, we adopted the soft Voronoi potential defined in ref 39. The only parameter of the Voronoi potential, which is the distance from the atomic centers to the switch-on-edge of the CAP, $r_{cut}$, was set to 3.0 Bohr for formaldehyde and 4.0 Bohr for chloroethene and $N_2$. Systematic examinations regarding this parameter were performed previously, and only a very mild dependence of the resonance energy was found. Yet, for $r_{cut}$ values in the chosen parameter range, the most pronounced stabilizations of the $\eta$-trajectories were obtained.[40,41]

All CAP/SAC-CI calculations were done with the Gaussian 09 package.[55] The CAP/XMS-CASPT2 calculations were performed with the orz program package.[43] In all SAC-CI and CASPT2 calculations, all core electrons were kept frozen. We analyze the role of the basis set size by employing two Dunning basis sets cc-pV$n$Z ($n$ = D, T).[47,56] The basis sets of all nonhydrogen atoms were further augmented with even-tempered diffuse functions contracted to [2s5p2d].[22] In the CASPT2 calculations, we used an IPEA shift[29] of 0.25 au and an imaginary shift[30] of 0.1 au to avoid intruder states.

## RESULTS AND DISCUSSION

**$^2B_1$ Resonance of Formaldehyde Anion.** The electronic structure of formaldehyde is ...$(5a_1)^2(1b_1)^2(2b_2)^2$. When formaldehyde captures one electron, this electron occupies a $b_1$ virtual orbital, forming a $^2B_1$ $\pi^*$ resonance. This resonance has been experimentally characterized by its electron transmission spectrum (ETS)[57,58] and vibrational excitation spectrum[59] and computationally studied with numerous methods (see Table 1). It can be seen that different theoretical methods give different results, for example, $E_r$ varies widely from 0.7 to 1.5 eV. All SAC-CI and EOM-CCSD-based methods predict more consistent $E_r$ values in the range 1.1−1.3

**Table 1. Resonance Position $E_r$ and Width Γ (in eV) of the $^2B_1$ Resonance of $H_2CO^-$ Calculated with Different Methods**

| method | $E_r$ (eV) | Γ (eV) |
|---|---|---|
| experiment | | |
| electron transmission spectroscopy[a] | 0.86[o], 0.65[p] | |
| vibrational excitation[b] | 0.87[o] | |
| calculated | | |
| complex Kohn[c] | ∼1.0 | ∼0.5 |
| dilated electron propagator[d] | 0.89−1.0 | 0.10−0.12 |
| $R$-matrix | 1.32[e], 1.46[f] | 0.55[e], 0.79[f] |
| finite-element-discrete-model[g] | 0.682 | 0.429 |
| CAP/EOM-EA-CCSD (1st order)[h] | 1.314 | 0.277 |
| CIP-FSMRCC[i] | 0.76 | 0.32 |
| CAP/SAC-CI[j] | 1.119 | 0.462 |
| CAP/SAC-CI[k] | 1.191 | 0.414 |
| CAP/XMS-CASPT2[k,l,m] | 1.173 | 0.395 |
| CAP/XMS-CASPT2[k,l,n] | 1.266−1.279 | 0.470−0.483 |

[a]References 57 and 58. [b]Reference 59. [c]Reference 60. [d]Reference 61. [e]Reference 62. [f]Reference 63. [g]Reference 64. [h]Reference 25, aug-cc-pVTZ + [3s3p3d(C)] diffuse functions. [i]Reference 65, double-ζ basis set + [4p1d/1p] diffuse functions. [j]Reference 22, cc-pVTZ + [2s5p2d/2s2p] diffuse functions. [k]This work, cc-pVTZ + [2s5p2d] diffuse functions. [l]Results at the largest $n_{virt}$ values. [m]CAS(0,0) + 17 active space. [n]Range of CAS(2,2), CAS(4,3), and CAS(6,5) results. [o]Vertical electron affinity. [p]Adiabatic electron affinity.


https://dx.doi.org/10.1021/acs.jctc.9b01032
J. Chem. Theory Comput. 2020, 16, 2606−2616

eV. Most methods tend to overestimate $E_r$ as compared to the experimental values of 0.65 eV (adiabatic) and 0.86 eV (vertical). It is clear that the adiabatic attachment energy is considerably lower than the vertical value[22] and that the experimentally observed progression is therefore broad and that the intensities of each vibrational state are impacted not only by Franck−Condon factors but also by their lifetimes. Thus, only a model of the ETS or electron impact vibrational excitation spectrum can be directly compared with experiment.

As mentioned above, we will study the impact of two factors (i) the basis set size and more importantly, (ii) the choice of active space controlled by the CAS($n_e$,$n_o$) active space and $n_{virt}$. All CAP/XMS-CASPT2 results can be found in Figures 2 and 3 as well as Tables S1 and S2.

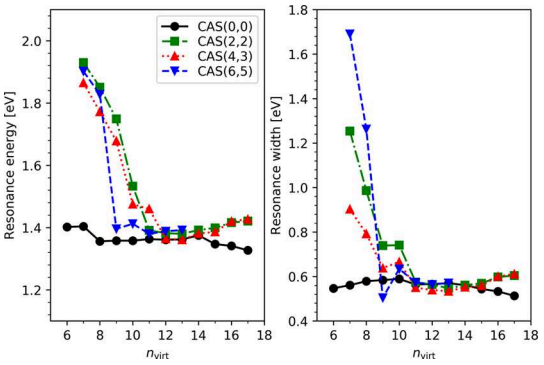


**Figure 2.** Resonance position $E_r$ and width Γ (in eV) of the $\pi^*$ $^2B_1$ resonance of $H_2CO^-$, calculated with different CAS($n_e$,$n_o$) + $n_{virt}$, cc-pVDZ + [2s5p2d] diffuse functions.

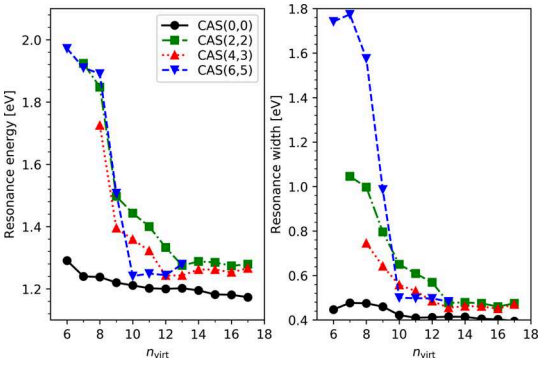


**Figure 3.** Resonance position $E_r$ and width Γ (in eV) of the $\pi^*$ $^2B_1$ resonance of $H_2CO^-$, calculated with different CAS($n_e$,$n_o$) + $n_{virt}$, cc-pVTZ + [2s5p2d] diffuse functions.

We first focus on the results calculated with the cc-pVDZ + [2s5p2d] basis set (Figure 2). It can be seen that $n_{virt}$ is a crucial factor determining the accuracy of the calculations and governing whether the resonance could be found from the $\eta$-trajectories. For instance, if $n_{virt}$ is not sufficiently large ($n_{virt} \leq 5$), we failed to locate the resonance state. With the CAS(0,0) active space, we observed a weak dependence of $E_r$ and Γ on $n_{virt}$. At the smallest $n_{virt}$ = 6, $E_r$ = 1.402 eV and Γ = 0.547 eV, being in good agreement with the values calculated at the largest $n_{virt}$ ($E_r$ = 1.327 eV and Γ = 0.513 eV). In contrast, the larger active spaces yield results depending strongly on $n_{virt}$. For example, using a small $n_{virt}$ in combination with CAS(6,5) can cause an error of ∼0.5 eV for $E_r$ and up to ∼1 eV for Γ. Satisfactory results are achieved only at larger $n_{virt}$ values (≥13).

It is not trivial to explain the markedly different convergence behaviors of $E_r$ with respect to $n_{virt}$ between CAS(0,0) and the larger active spaces. In the former case, we expect that the results primarily depend on the nature (shape and eigenvalue) of $n_{virt}$ $b_1$ virtual orbitals. Upon expanding the CAS(0,0) with the ($\pi_{CO}$, $\pi^*_{CO}$) pair belonging to the $b_1$ irrep, all $b_1$ virtual orbitals are "perturbed". This perturbation is correlated to the large difference between CAS(0,0) and CAS(2,2) results at small $n_{virt}$. In contrast, going from CAS(2,2) to CAS(4,3) or CAS(6,5), only orbitals belonging to either $a_1$ or $b_2$ irrep were added. The perturbation of these orbitals to the $b_1$ virtual space is certainly minimal; consequently, we found similar convergence behaviors between CAS(2,2), CAS(4,3), and CAS(6,5).

Despite having different convergence behaviors, all four active spaces predict fairly similar results at the largest $n_{virt}$ value: $E_r$ = 1.327−1.427 eV and Γ = 0.513−0.611 eV. Such similar predictions are attributed to the fact that the wave function of formaldehyde at its equilibrium geometry is already well characterized at the HF level. This behavior can in general be expected in molecules with negligible static electron correlation, and for shape resonances of such molecules the size-extensive methods CAP/SAC-CI or CAP/EOM-EA-CCSD have an advantage.

We now briefly discuss the effect of the basis set size (double-ζ vs triple-ζ) on the results (see Figures 2 and 3). We only consider the data at the largest $n_{virt}$. In agreement with the previous CAP/SAC-CI work, it turned out that the size of the valence basis set is less critical than the size of the diffuse basis set.[22] We found that with CAP/XMS-CASPT2, going from double to triple-ζ quality reduces the resonance position by 0.11−0.16 eV and narrow the width by 0.09−0.14 eV. The reduction of the computed resonance position can be explained in terms of the anion benefitting more than the neutral molecule from increasing the valence basis set size.[22]

We finally compare the CAP/XMS-CASPT2 data to the results calculated with different CAP-augmented methods and the experimental data. Because the formaldehyde $^2B_1$ resonance is a single-reference case, we expect that CAP/SAC-CI, CAP/EOM-CCSD, and CAP/XMS-CAS methods yield comparable results. Indeed, all these methods agree with each other to within 0.2 eV. While CAP/SAC-CI predicts $E_r$ = 1.191 eV and Γ = 0.414 eV, CAP/XMS-CAS(0,0) + 17-PT2 predicts slightly smaller $E_r$ and Γ values of 1.173 and 0.395 eV, respectively. On the other hand, the larger active spaces systematically give larger resonance energies and widths, 1.266−1.279 and 0.470−0.483 eV, respectively. All results are in good agreement with the data reported by Zuev et al.,[25] adopting CAP/EOM-EA-CCSD (1.314 and 0.277 eV for $E_r$ and Γ, respectively). As compared with the experiment, all recent CAP calculations overestimate $E_r$ by 0.44 eV (CAP/EOM-EA-CCSD), 0.32 eV (CAP/SAC-CI), and 0.3−0.4 eV (CAP/XMS-CASPT2).

**$\sigma^*$ and $\pi^*$ Resonance States of Chloroethene Anion.** The dissociative electron attachment (DEA) process, AB + $e^-$ → $[AB^-]^*$ → A + $B^-$, in unsaturated chlorohydrocarbons has been the subject of study in numerous experimental and theoretical studies.[66−78] It has been proposed that the dissociation mechanism of this class of compound involves the initial formation of a relatively long lived $\pi^*$ resonance and subsequent coupling with a $\sigma^*$ resonance that promotes the


https://dx.doi.org/10.1021/acs.jctc.9b01032
J. Chem. Theory Comput. 2020, 16, 2606−2616

dissociation of the C−Cl bond,[73] but is only short-lived in the vicinity of the equilibrium geometry. However, it has been pointed out that this mechanism will compete with direct formation of the $\sigma^*$ resonance.[79]

Here, chloroethene is studied to test the new method combination, and we start by calculating the $\sigma^*$ and $\pi^*$ resonances, which are $^2A'$ and $^2A''$ states in $C_s$ symmetry, using CAP/XMS-CASPT2 and CAP/SAC-CI. The experimental resonance positions, as well as previously reported and our current theoretical results are summarized in Table 2.

**Table 2. Resonance Position $E_r$ (in eV) of the $\sigma^*$ and $\pi^*$ Resonances of $CH_2CHCl^-$ Calculated with Different Methods**

| method | $\sigma^*$ (eV) | $\pi^*$ (eV) |
|---|---|---|
| experiment | | |
| electron transmission spectroscopy[a,b] | 2.84 | 1.28 |
| calculated | | |
| CAP/ADC(2)[c] | 2.36 | 1.59 |
| CAP/EOM-EA-CCSD[d] | | 1.730 |
| CAP/SAC-CI[e] | 2.530 | 1.718 |
| CAP/XMS-CASPT2 | ~2.65[f] | 1.810[g] |

[a]Reference 73. [b]Reference 72. [c]Reference 66, cc-pVDZ + [1s8p2d1f] basis set. [d]Reference 78, aug-cc-pVTZ + 3p basis set. [e]This work, cc-pVDZ + [2s5p2d] basis set. [f]Estimated, based on the CAP/SAC-CI result, see text. [g]CAS(2,2) + 10.

In CAP/XMS-CASPT2 calculations, we used two CAS-($n_e$,$n_o$) active spaces: CAS(0,0) and CAS(2,2) (see also Figure S1). The CAS(2,2) active space represents the minimal active space to correctly describe the multireference character of the wave function upon dissociation of the C−Cl bond. On top of each CAS($n_e$,$n_o$), we included 10 $a''$ or 17 $a'$ virtual orbitals in the calculations of the $\pi^*$ and $\sigma^*$ resonances, respectively. Yet, unfortunately, we were unable to clearly identify the $\sigma^*$ resonance in all CAS(2,2) + 17 and in two CAS(0,0) + 17 calculations. This is a known problem; as a rule, $\sigma^*$ resonances have large widths and stabilize therefore much further from the real axis than $\pi^*$ resonances. One can—as a rule—identify the resonance trajectory, but, again—as a rule—the resonance trajectory tends to show no or only weak stabilizations. Two strategies could be adopted to alleviate this problem. The straightforward one is to include more diffuse orbitals in the active space. However, this drastically increases the computational cost. A more efficient way is to manually select a set of virtual orbitals based on preliminary calculations at a lower computational level, such as CIS, as suggested by Kunitsa et al.[26] This strategy, however, introduces a certain bias and does by no means guarantee that the resonance trajectory will show a clear stabilization.

The resonance positions and widths at different $d$(C−Cl) values are shown in Figure 4. Numerical results can be found in Tables S3 and S4. We first compare the results of SAC-CI and XMS-CASPT2 using the CAS(0,0) + $n_{virt}$ active space. Both methods give similar $E_r$ results (with differences of 0.1−0.2 eV) and predict that the resonance positions decrease when increasing the C−Cl bond distance. Moreover, SAC-CI systematically produces smaller $E_r$ values as compared to XMS-CASPT2 around the equilibrium structure ($d$(C−Cl) = 1.75−2.10 Å). For the resonance widths Γ, both methods predict comparable results with differences of less than 0.05 eV in most cases and of 0.11 eV in the worst-case scenario.

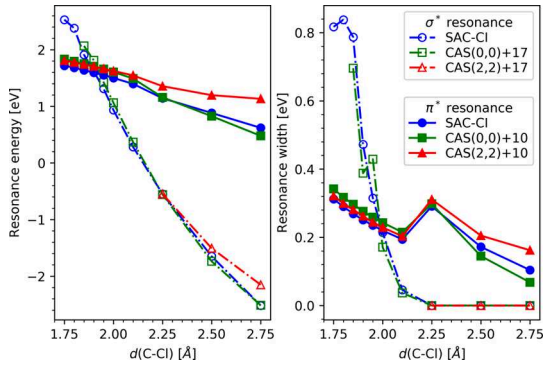


**Figure 4.** Resonance position $E_r$ and width Γ (in eV) of the $\sigma^*$ and $\pi^*$ resonances of chloroethene anion, calculated with CAP/SAC-CI and CAP/XMS-CASPT2. At $d$(C−Cl) > 2.10 Å, the $\sigma^*$ resonance disappears ($E_r$ < 0 and Γ = 0).

We now turn to a comparison between the CAS(0,0) + $n_{virt}$ and CAS(2,2) + $n_{virt}$ active spaces. As we failed to identify the $\sigma^*$ resonance in the CAS(2,2) + 17 calculations, we discuss here only the $\pi^*$ resonance. Based on the multireference character of the wave function provided in Table S6, we expect that the two active spaces should give almost identical resonance positions and widths at short C−Cl bond distances. Indeed, the differences are less than 0.02 eV for $d$(C−Cl) = 1.75−2.00 Å. At distances longer than 2.10 Å, however, the multireference character increases, and consequently, CAS(0,0) is expected to perform more and more poorly. Practically, CAS(0,0) systematically underestimates the $\pi^*$ resonance positions as compared to the results produced by the CAS(2,2) active space, and at the longest bond distance (2.75 Å), its error has grown to 0.65 eV. Also, the resonance width predicted by CAS(0,0) at this distance is too small (0.07 eV) as compared to the CAS(2,2) value (0.16 eV).

In Figure 5, we plot the PECs of the GS of the neutral molecule, as well as the $\sigma^*$ and $\pi^*$ resonances of the anion

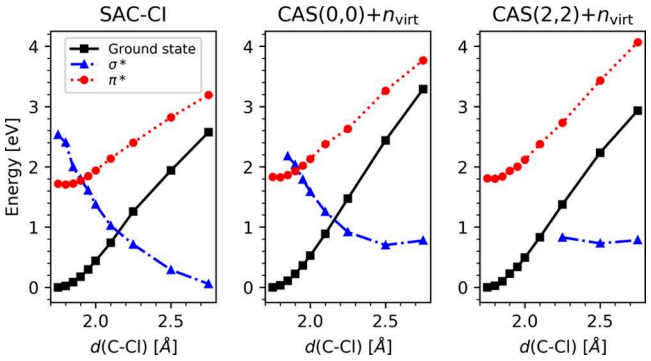


**Figure 5.** PECs of the GS of the neutral molecule, $\sigma^*$, and $\pi^*$ resonances of the anion calculated with SAC-CI and XMS-CASPT2. $n_{virt}$ = 10 and 17 for $\sigma^*$ and $\pi^*$ resonances, respectively.

along the bond stretching coordinate $d$(C−Cl). We use the total energy of the GS at the equilibrium structure as a reference. We focus on the results around the equilibrium where the two resonance PECs cross. As discussed above, because the wave function around this point is well described by HF, CAP/SAC-CI and CAP/XMS-CASPT2 results are in excellent agreement with each other. They both predict that (i) the $\sigma^*$ and $\pi^*$ curves cross at $d$(C−Cl) ≈ 1.9 Å and (ii) the $\sigma^*$ resonance disappears at $d$(C−Cl) > 2.15 Å. This one-


https://dx.doi.org/10.1021/acs.jctc.9b01032
J. Chem. Theory Comput. 2020, 16, 2606−2616

Table 3. Wavefunction of Different States of $N_2$ and $N_2^-$ Calculated with CASSCF(6,6) at $d$ = 1.30 Å

| molecule | state | $D_{2h}$ irrep | dominant determinant[a] | coefficient | weight |
|---|---|---|---|---|---|
| $N_2$ | $A^3\Sigma_u^+$ | $^3B_{1u}$ | $\|(\sigma_g)^2(\pi_{ux})^2(\pi_{uy})^{\uparrow}(\pi_{gx}^*)^{\uparrow}(\pi_{gy}^*)^0\rangle$ | 0.676 | 0.457 |
| | | | $\|(\sigma_g)^2(\pi_{ux})^{\uparrow}(\pi_{uy})^2(\pi_{gx}^*)^0(\pi_{gy}^*)^{\uparrow}\rangle$ | 0.676 | 0.457 |
| | $W^3\Delta_u$ | $^3A_u$ | $\|(\sigma_g)^2(\pi_{ux})^{\uparrow}(\pi_{uy})^2(\pi_{gx}^*)^{\uparrow}(\pi_{gy}^*)^0\rangle$ | 0.685 | 0.470 |
| | | | $\|(\sigma_g)^2(\pi_{ux})^2(\pi_{uy})^{\uparrow}(\pi_{gx}^*)^0(\pi_{gy}^*)^{\uparrow}\rangle$ | 0.685 | 0.470 |
| | $W^3\Delta_u$ | $^3B_{1u}$ | $\|(\sigma_g)^2(\pi_{ux})^2(\pi_{uy})^{\uparrow}(\pi_{gx}^*)^{\uparrow}(\pi_{gy}^*)^0\rangle$ | 0.685 | 0.470 |
| | | | $\|(\sigma_g)^2(\pi_{ux})^{\uparrow}(\pi_{uy})^2(\pi_{gx}^*)^0(\pi_{gy}^*)^{\uparrow}\rangle$ | −0.685 | 0.470 |
| $N_2^-$ | $^4\Pi_u$ | $^4B_{3u}$ | $\|(\sigma_g)^2(\pi_{ux})^2(\pi_{uy})^{\uparrow}(\pi_{gx}^*)^{\uparrow}(\pi_{gy}^*)^{\uparrow}\rangle$ | 0.989 | 0.979 |
| | $^4\Pi_u$ | $^4B_{2u}$ | $\|(\sigma_g)^2(\pi_{ux})^{\uparrow}(\pi_{uy})^2(\pi_{gx}^*)^{\uparrow}(\pi_{gy}^*)^{\uparrow}\rangle$ | 0.989 | 0.979 |
| | $^2\Pi_u$ | $^2B_{2u}$ | $\|(\sigma_g)^2(\pi_{ux})^{\downarrow}(\pi_{uy})^2(\pi_{gx}^*)^{\uparrow}(\pi_{gy}^*)^{\uparrow}\rangle$ | 0.499 | 0.249 |
| | | | $\|(\sigma_g)^2(\pi_{ux})^{\uparrow}(\pi_{uy})^2(\pi_{gx}^*)^{\downarrow}(\pi_{gy}^*)^{\uparrow}\rangle$ | 0.610 | 0.372 |
| | | | $\|(\sigma_g)^2(\pi_{ux})^2(\pi_{uy})^{\uparrow}(\pi_{gx}^*)^2(\pi_{gy}^*)^0\rangle$ | 0.559 | 0.313 |
| | $^2\Pi_u$ | $^2B_{3u}$ | $\|(\sigma_g)^2(\pi_{ux})^2(\pi_{uy})^{\downarrow}(\pi_{gx}^*)^{\uparrow}(\pi_{gy}^*)^{\uparrow}\rangle$ | 0.499 | 0.249 |
| | | | $\|(\sigma_g)^2(\pi_{ux})^2(\pi_{uy})^{\uparrow}(\pi_{gx}^*)^{\uparrow}(\pi_{gy}^*)^{\downarrow}\rangle$ | 0.610 | 0.372 |
| | | | $\|(\sigma_g)^2(\pi_{ux})^{\uparrow}(\pi_{uy})^2(\pi_{gx}^*)^0(\pi_{gy}^*)^2\rangle$ | 0.559 | 0.313 |

[a]Core orbital = $(1\sigma_g)^2(1\sigma_u)^2(2\sigma_g)^2(2\sigma_u)^2$.

dimensional cut through the multidimensional crossing cone is consistent with earlier studies of the DEA mechanism.[73]

It is also interesting to discuss the PECs at larger bond distances. The results produced by CAS(2,2) + $n_{virt}$ should be more reliable than those of SAC-CI and CAS(0,0) + $n_{virt}$. Neither of the latter two can fully reproduce the CAS(2,2) + $n_{virt}$ PECs for long bond lengths. For example CAS(0,0) + $n_{virt}$ moderately overbinds the C−Cl bond due to its intrinsic failure of describing bond dissociation, whereas SAC-CI predicts a too steep $\sigma^*$ curve.

Finally, it is noteworthy to compare our results at the equilibrium geometry to previously reported results and the experimental data. We crudely estimate the $\sigma^*$ resonance position at the CAS(0,0) + 17 level to be ∼2.65 eV (see Table 2). This crude estimation is based on the CAP/SAC-CI value (2.53 eV) and on the observation that CAP/SAC-CI gives smaller $E_r$ values than CAS(0,0) + 17 by ∼0.15 eV (vide supra). Again, all recent CAP-based methods predict similar results to within 0.3 eV. As compared to the experimental data, the accuracies are acceptable. All methods systematically underestimate the $\sigma^*$ resonance position by 0.2−0.5 eV and overestimate the $\pi^*$ resonance position by 0.3−0.5 eV. Such different deviations have been discussed in detail in the previous work of Feuerbacher et al.[66]

**$^4\Pi_u$ and $^2\Pi_u$ Resonance States of $N_2^-$.** The $N_2^-$ anion has been the subject of numerous experimental and theoretical studies.[18,20,25,26,80−89] Most work focused on the $^2\Pi_g$resonance $(1\sigma_g)^2(1\sigma_u)^2(2\sigma_g)^2(2\sigma_u)^2(1\pi_u)^4(3\sigma_g)^2(1\pi_g^*)^1$, a well-known shape-type resonance having very short lifetimes.[80] On the other hand, much longer-lived (at least 10 $\mu$s) resonance states have been experimentally observed.[89,90] Based on CCSD(T) calculations, Sommerfeld and Cederbaum[91] initially proposed the $^4\Pi_u$ resonance state as a candidate for the observed long-lived state. This state has an electronic configuration $(1\sigma_g)^2(1\sigma_u)^2(2\sigma_g)^2(2\sigma_u)^2(1\pi_u)^3(3\sigma_g)^2(1\pi_g^*)^2$ and it can be thought of as a $\pi_u \rightarrow \pi_g^*$ excitation of the $^2\Pi_g$ shape resonance or as formed by electron attachment to either the $A^3\Sigma_u^+$ or the $W^3\Delta_u$ triplet states of $N_2$, which are both described by the configuration $(1\sigma_g)^2(1\sigma_u)^2(2\sigma_g)^2(2\sigma_u)^2(1\pi_u)^3(3\sigma_g)^2(1\pi_g^*)^1$. At the CCSD(T) level of theory, the $^4\Pi_u$ state turns out to be a long-lived resonance state (with a lifetime of about $2 \times 10^{-12}$ s) and it is stable with respect to vertical autodetachment to the $A^3\Sigma_u^+$ by 0.28 eV. However, in a joint experimental and theoretical work later, Andersen et al.[92] provided evidence that the long-lived $N_2^-$ species should be rather attributed to the $^6\Sigma_u^+$ and $^6\Pi_u^+$ sextet states with decay into the $^5\Sigma_g^+$ parent state.

One problem plaguing the CCSD(T) study from the onset is that the $^3\Sigma_u^+$ triplet state of $N_2$ exhibits strong multireference character, rending the CCSD(T) curve crossing unreliable. Indeed, the wave function of this state around the equilibrium geometry is qualitatively described as a mixture of two determinants $[\text{core}]^8(3\sigma_g)^2(1\pi_{ux})^2(1\pi_{uy})^1(1\pi_{gx}^*)^1(1\pi_{gy}^*)^0$ and $[\text{core}]^8(3\sigma_g)^2(1\pi_{ux})^1(1\pi_{uy})^2(1\pi_{gx}^*)^0(1\pi_{gy}^*)^1$ (see also Table 3). Thus, this state can be best described using multireference approaches such as CASSCF/CASPT2.

Here, the PECs of the $^4\Pi_u$ and $^2\Pi_u$ resonances are investigated as the first real test for the CAP/XMS-CASPT2 method. In particular, the doublet state has not been described in the literature before and represents a challenge because both the resonance and the parent show strong multireference character (see Table 3).

The CAP/XMS-CASPT2 PECs of the $^3\Sigma_u^+$ and $^3\Delta_u$ parent states of $N_2$, as well as the $^4\Pi_u$ and $^2\Pi_u$ resonance states of $N_2^-$, are shown in Figure 6. The equilibrium bond lengths of the $^3\Delta_u$ and $^3\Sigma_u^+$ states predicted by CAP/XMS-CASPT2 are 1.282 and 1.292 Å, respectively. Both results are in good

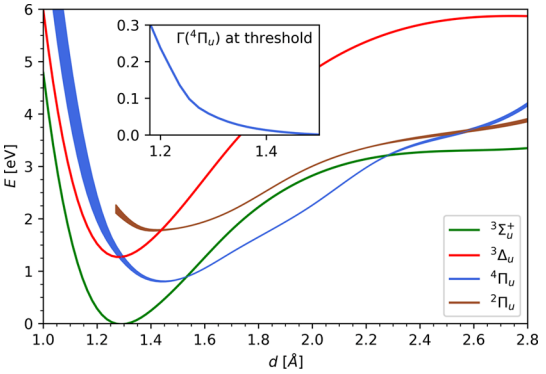


Figure 6. PECs (in eV) of the $^3\Sigma_u^+$ and $^3\Delta_u$ states of $N_2$; and the $^4\Pi_u$ and $^2\Pi_u$ resonance states of $N_2^-$, calculated with CAP/XMS-CASPT2, $n_{virt}$ = 10, cc-pVTZ + [2s5p2d] basis set. The minimum of the $^3\Sigma_u^+$ state is used as the reference. The resonance width (Γ) of the $^4\Pi_u$ and $^2\Pi_u$ resonance states is represented as the line width of the curve. For $d$ = 1.53−2.28 Å, $\Gamma(^4\Pi_u)$ is 0.



https://dx.doi.org/10.1021/acs.jctc.9b01032
J. Chem. Theory Comput. 2020, 16, 2606−2616

agreement with the experimental values of 1.278 and 1.287 Å, respectively.[93] The $^4\Pi_u$ and $^2\Pi_u$ resonance states have significantly longer equilibrium bond lengths (1.444 and 1.402 Å, respectively) due to the occupation of the antibonding $\pi_g^*$ orbitals. The CAP/XMS-CASPT2 equilibrium bond length of $^4\Pi_u$ is quite close to the values calculated with CCSD(T)[91] and third-order many-body perturbation theory,[92] that is, 1.430 and 1.44 Å, respectively.

The results shown in Figure 6 clearly indicate that the $^2\Pi_u$ state is unstable with respect to the $^3\Sigma_u^+$ state at all geometries, whereas it crosses the $^3\Delta_u$ state at $d$ = 1.44 Å and is unstable to both decay channels at small bond lengths only. Accordingly, its width is always positive, fairly large at short bond distances (up to 0.6 eV at $d$ = 1.28 Å), but rapidly decreases after crossing the $^3\Delta_u$ state (see also Figure S3). Thus, the $^2\Pi_u$ state represents a so-called core-excited shape resonance, and we predict its lifetime to be short.

As compared to the doublet state, the $^4\Pi_u$ state turns out to be a different story entirely. First, it is much more stable, leading to three crossing points at $d$ = 1.53 and 2.28 Å with the $^3\Sigma_u^+$ state and at $d \approx$ 1.30 Å with the $^3\Delta_u$ state. Unsurprisingly, CAP/XMS-CASPT2 predicts the triplet states significantly stabilized in respect with the quartet state, and in contrast to CCSD(T),[91] the adiabatic electron affinity is −0.8 eV, and the $^4\Pi_u$ state is unstable with respect to vertical autodetachment by 0.37 eV. Along the PEC, the quartet state changes its character: between 1.53 and 2.28 Å it is a Feshbach resonance, outside this range it is a core-excited shape resonance. As it has core-excited-shape resonance character at its equilibrium geometry, all vibrational states are expected to be short-lived.

Second, we consider the close correlation between the $^4\Pi_u$ PEC and its width, which suggests that even though CAP/XMS-CASPT2 is formerly not size extensive, for all practical purposes it is. While for $d$ > 2.28 Å, the $^4\Pi_u$ state is less stable than the $^3\Sigma_u^+$ state, and $\Gamma(^4\Pi_u)$ possesses accordingly a finite value, for $d$ = 1.53−2.28 Å, the $^4\Pi_u$ state is more stable than both triplet states, and $\Gamma(^4\Pi_u)$ must vanish, which it does (see inset in Figures 6 and S2). At $d$ = 1.53 Å, the $^4\Pi_u$ state recrosses the $^3\Sigma_u^+$ state, reopening the $N_2^-(^4\Pi_u) \rightarrow N_2(^3\Sigma_u^+) + e^-$ decay channel and $\Gamma(^4\Pi_u)$ increases slowly. Finally, the decay channel $N_2^-(^4\Pi_u) \rightarrow N_2(^3\Delta_u) + e^-$ opens at $d$ = 1.30 Å, leading to a steep increase in $\Gamma(^4\Pi_u)$ as a function of $d$ (see inset in Figure 6). As the curve crossings perfectly reflect the positions at which $\Gamma$ vanishes, we conclude that the balance requirement between the parent and the resonance state as well as the internal balance requirement in the resonance wavefunction is satisfied to the extent noticeable on the scales of our Figures.

## SUMMARY

We have introduced a combination of a Voronoi CAP with the XMS-CASPT2 method, which has been implemented in our own XMS-CASPT2 code.[43] The corrected $\eta$-trajectories of the present approach provided stable resonance energy in most cases; however, for certain CAS spaces, $\sigma^*$ resonances could not be clearly identified, and finding a reliable method for $\sigma^*$ resonances remains an open question.

Benchmark calculations were performed for the $\pi^*$ resonance state of formaldehyde. The CAP/XMS-CASPT2 method provided vertical resonance energy and width in excellent agreement with SAC-CI- and EOM-CCSD-based methods. Extension of the CAS was systematically studied, and it was shown that even small CAS spaces provide very good results. Using just HF (CAS(0,0)) and therefore effectively MP2 yields reasonable results compared to SAC-CI or EOM-CCSD.

The new method was also applied to the PECs of the $\pi^*$ and $\sigma^*$ resonance states of chloroethene along the C−Cl bond dissociation coordinate. The CAP/XMS-CASPT2 results again agree well with those obtained using CAP/SAC-CI, yielding systematically lower resonance energies by about 0.15 eV than CAP/SAC-CI—at least for this system—a fact used for the estimation of the $\sigma^*$ resonance energy at the equilibrium geometry. This estimation was unfortunately needed, because CAP/XMS-CASPT2 seems to be slightly less robust regarding the quality of the produced $\eta$-trajectories, that is, although the resonance trajectories can be identified, neither the trajectories nor the corrected trajectories show a pronounced stabilization behavior. While the lack of stabilization may be considered to represent a curse for the new method as is, CAP/XMS-CASPT2 contains in a sense its own cure: it is much more flexible than, say, CAP/SAC-CI, and now that we identified a reproducible failure, it can hopefully be addressed, by some unbiased and computationally efficient scheme to select better virtual orbitals for the CAP Hamiltonian.

The advantage of CAP/XMS-CASPT2 was clearly demonstrated in the calculations of the PECs of the $^4\Pi_u$ and $^2\Pi_u$ resonance states of $N_2^-$. Here, the parent states, $A\ ^3\Sigma_u^+$ and $W\ ^3\Delta_u$, as well as the $^2\Pi_u$ resonance state show pronounced multireference character, HF fails to provide an adequate description of the situation, and even relative energies obtained with CCSD(T) cannot be trusted.

In conclusion, in this pilot work of CAP/XMS-CASPT2, we have demonstrated the pros and cons of the method to study different types of resonance states. Although it can be useful to study resonances states having substantial multireference character, some difficulties related to choosing active virtual orbitals have been found, hindering its usage (at least in a black-box manner). A promising way to overcome these issues is to improve the description of the virtual active orbitals, using the extended Koopmans' theorem.[94] It is unclear, however, whether this will completely solve the impracticality issue in the present form, that is, choosing which and how many orbitals should be in the active space. Moreover, in larger molecules and molecules without point group symmetry, the problem of locating stable resonances will be certainly much more difficult; thus, improving the virtual orbitals may not be a realistic solution. A promising alternative would be some type of SAC-CI like linear response theory in a multireference framework.

## ASSOCIATED CONTENT

### Supporting Information

The Supporting Information is available free of charge at https://pubs.acs.org/doi/10.1021/acs.jctc.9b01032.

Resonance position $E_r$ and width $\Gamma$ of the $^2B_1$ resonance of $H_2CO^-$, $\pi^*$, and $\sigma^*$ resonances of $CH_2CHCl^-$, calculated with CAP/SAC-CI and CAP/XMS-CASPT2; resonance position $E_r$ and width $\Gamma$ of the $^4\Pi_u$ and $^2\Pi_u$ resonances of $N_2^-$, calculated with CAP/XMS-CASPT2; weight of the leading configuration $w$ and natural orbital occupation number (NOON) in the CASSCF calculations of $CH_2CHCl$; CAS(2,2) active space used in the calculations of $CH_2CHCl$; $\eta$-trajectories of the $\pi^*$ and



https://dx.doi.org/10.1021/acs.jctc.9b01032
J. Chem. Theory Comput. 2020, 16, 2606−2616

$\sigma^*$ resonances of $CH_2CHCl^-$ at different C−Cl bond distances; and cartesian coordinates of $H_2CO$ and $CH_2CHCl$ (PDF)

## AUTHOR INFORMATION


### Corresponding Authors

**Takeshi Yanai** − *Institute of Transformative Bio-Molecules (WPI-ITbM) and Department of Chemistry, Graduate School of Science, Nagoya University, Nagoya, Aichi 464-8602, Japan; Japan Science and Technology Agency, PRESTO, Kawaguchi, Saitama 332-0012, Japan*; Email: yanait@chem.nagoya-u.ac.jp

**Thomas Sommerfeld** − *Department of Chemistry and Physics, Southeastern Louisiana University, Hammond, Louisiana 70402, United States*; orcid.org/0000-0001-8105-5414; Email: thomas.sommerfeld@selu.edu

**Masahiro Ehara** − *Institute for Molecular Science and Research Center for Computational Science, Okazaki 444-8585, Japan; Elements Strategy Initiative for Catalysts and Batteries (ESICB), Kyoto University, Kyoto 615-8520, Japan*; orcid.org/0000-0002-2185-0077; Email: ehara@ims.ac.jp

### Authors

**Quan Manh Phung** − *Institute of Transformative Bio-Molecules (WPI-ITbM), Nagoya University, Nagoya, Aichi 464-8602, Japan*; orcid.org/0000-0001-8205-5328

**Yuki Komori** − *Department of Chemistry, Graduate School of Science, Nagoya University, Nagoya, Aichi 464-8602, Japan*

Complete contact information is available at: https://pubs.acs.org/10.1021/acs.jctc.9b01032


### Notes

The authors declare no competing financial interest.

## ACKNOWLEDGMENTS

This work was supported by the financial support from a Grant-in-Aid for Scientific Research, Japan Society for the Promotion of Science (JSPS), JP16H04104 and JP16H06511 (M.E.), and by JST, PRESTO Grant Number 17937609 (T.Y.). M.E. acknowledges a MEXT program (Ministry of Education Culture, Sports, Science and Technology in Japan) "Elements Strategy Initiative to Form Core Research Center." T.S. acknowledges the support by the National Science Foundation under Grant CHE-1565495. The computations were partially performed at the Research Center for Computational Science, Okazaki, Japan.

## REFERENCES


(1) Jordan, K. D.; Burrow, P. D. Temporary Anion States of Polyatomic Hydrocarbons. *Chem. Rev.* **1987**, *87*, 557−588.

(2) Sommerfeld, T. Lifetimes of Metastable Dianions: $CN_2^{2-}$, $C_4^{2-}$, and $CO_3^{2-}$. *J. Phys. Chem. A* **2000**, *104*, 8806−8813.

(3) Thompson, M.; Baker, M. D.; Christie, A.; Tyson, J. F. *Auger Electron Spectroscopy*; John Wiley: New York, 1985.

(4) Santra, R.; Zobeley, J.; Cederbaum, L. S.; Tarantelli, F. Intermolecular Coulombic Decay of Clusters. *J. Electron Spectrosc. Relat. Phenom.* **2001**, *114-116*, 41−47.

(5) Mason, N. J. Electron-Induced Chemistry: A Forward Look. *Int. J. Mass Spectrom.* **2008**, *277*, 31−34.

(6) Davis, D.; Vysotskiy, V. P.; Sajeev, Y.; Cederbaum, L. S. Electron Impact Catalytic Dissociation: Two-Bond Breaking by a Low-Energy Catalytic Electron. *Angew. Chem., Int. Ed.* **2011**, *50*, 4119−4122.

(7) Jolicard, G.; Austin, E. J. Optical Potential Stabilisation Method for Predicting Resonance Levels. *Chem. Phys. Lett.* **1985**, *121*, 106−110.

(8) Riss, U. V.; Meyer, H.-D. Calculation of Resonance Energies and Widths Using the Complex Absorbing Potential Method. *J. Phys. B: At., Mol. Opt. Phys.* **1993**, *26*, 4503−4535.

(9) Moiseyev, N. Quantum Theory of Resonances: Calculating Energies, Widths and Cross-Sections by Complex Scaling. *Phys. Rep.* **1998**, *302*, 212−293.

(10) Hazi, A. U.; Taylor, H. S. Stabilization Method of Calculating Resonance Energies: Model Problem. *Phys. Rev. A: At., Mol., Opt. Phys.* **1970**, *1*, 1109.

(11) Kukulin, V. I.; Krasnopol'sky, V. M. Description of Few-Body Systems via Analytical Continuation in Coupling Constant. *J. Phys. A: Math. Gen.* **1977**, *10*, L33.

(12) Horáček, J.; Paidarová, I.; Curík, R. On a Simple Way to Calculate Electronic Resonances for Polyatomic Molecules. *J. Chem. Phys.* **2015**, *143*, 184102.

(13) Sommerfeld, T.; Melugin, J. B.; Hamal, P.; Ehara, M. Resonance Energies and Lifetimes from the Analytic Continuation of the Coupling Constant Method: Robust Algorithms and a Critical Analysis. *J. Chem. Theory Comput.* **2017**, *13*, 2550−2560.

(14) Chao, J. S.-Y.; Falcetta, M. F.; Jordan, K. D. Application of the Stabilization Method to the $N_2^-(1\,^2\Pi_g)$ and $Mg^-(1\,^2P)$ Temporary Anion States. *J. Chem. Phys.* **1990**, *93*, 1125−1135.

(15) Sommerfeld, T.; Riss, U. V.; Meyer, H.-D.; Cederbaum, L. S.; Engels, B.; Suter, H. U. Temporary Anions - Calculation of Energy and Lifetime by Absorbing Potentials: the $N_2^-\,^2\Pi_g$ Resonance. *J. Phys. B: At., Mol. Opt. Phys.* **1998**, *31*, 4107−4122.

(16) Sommerfeld, T.; Tarantelli, F.; Meyer, H.-D.; Cederbaum, L. S. Ab Initio Calculation of Energies and Lifetimes of Metastable Dianions: the $C_2^{2-}$ Resonance. *J. Chem. Phys.* **2000**, *112*, 6635−6642.

(17) Sommerfeld, T. Resonance States of Atomic Di-anions. *Phys. Rev. Lett.* **2000**, *85*, 956−959.

(18) Sommerfeld, T.; Santra, R. Efficient Method to Perform CAP/CI Calculations for Temporary Anions. *Int. J. Quantum Chem.* **2001**, *82*, 218−226.

(19) Santra, R.; Cederbaum, L. S. Complex Absorbing Potentials in the Framework of Electron Propagator Theory. I. General Formalism. *J. Chem. Phys.* **2002**, *117*, 5511−5521.

(20) Feuerbacher, S.; Sommerfeld, T.; Santra, R.; Cederbaum, L. S. Complex Absorbing Potentials in the Framework of Electron Propagator Theory. II. Application to Temporary Anions. *J. Chem. Phys.* **2003**, *118*, 6188−6199.

(21) Sajeev, Y.; Pal, S. A General Formalism of the Fock Space Multireference Coupled Cluster Method for Investigating Molecular Electronic Resonances. *Mol. Phys.* **2005**, *103*, 2267−2275.

(22) Ehara, M.; Sommerfeld, T. CAP/SAC-CI Method for Calculating Resonance States of Metastable Anions. *Chem. Phys. Lett.* **2012**, *537*, 107−112.

(23) Ghosh, A.; Karne, A.; Pal, S.; Vaval, N. CAP/EOM-CCSD Method for the Study of Potential Curves of Resonant States. *Phys. Chem. Chem. Phys.* **2013**, *15*, 17915−17921.

(24) Jagau, T.-C.; Zuev, D.; Bravaya, K. B.; Epifanovsky, E.; Krylov, A. I. A Fresh Look at Resonances and Complex Absorbing Potentials: Density Matrix-Based Approach. *J. Phys. Chem. Lett.* **2014**, *5*, 310−315.

(25) Zuev, D.; Jagau, T.-C.; Bravaya, K. B.; Epifanovsky, E.; Shao, Y.; Sundstrom, E.; Head-Gordon, M.; Krylov, A. I. Complex Absorbing Potentials within EOM-CC Family of Methods: Theory, Implementation, and Benchmarks. *J. Chem. Phys.* **2014**, *141*, 024102.

(26) Kunitsa, A. A.; Granovsky, A. A.; Bravaya, K. B. CAP-XMCQDPT2 Method for Molecular Electronic Resonances. *J. Chem. Phys.* **2017**, *146*, 184107.

(27) Al-Saadon, R.; Shiozaki, T.; Knizia, G. Visualizing Complex-Valued Molecular Orbitals. *J. Phys. Chem. A* **2019**, *123*, 3223−3228.

(28) Finley, J.; Malmqvist, P.-Å.; Roos, B. O.; Serrano-Andrés, L. The Multi-state CASPT2 Method. *Chem. Phys. Lett.* **1998**, *288*, 299−306.

(29) Ghigo, G.; Roos, B. O.; Malmqvist, P.-Å. A Modified Definition of the Zeroth-Order Hamiltonian in Multiconfigurational Perturbation Theory (CASPT2). *Chem. Phys. Lett.* **2004**, *396*, 142−149.
(30) Forsberg, N.; Malmqvist, P.-Å. Multiconfiguration Perturbation Theory with Imaginary Level Shift. *Chem. Phys. Lett.* **1997**, *274*, 196−204.
(31) Andersson, K.; Malmqvist, P. A.; Roos, B. O.; Sadlej, A. J.; Wolinski, K. Second-Order Perturbation Theory with a CASSCF Reference Function. *J. Phys. Chem.* **1990**, *94*, 5483−5488.
(32) Andersson, K.; Malmqvist, P. Å.; Roos, B. O. Second-Order Perturbation Theory with a Complete Active Space Self-Consistent Field Reference Function. *J. Chem. Phys.* **1992**, *96*, 1218−1226.
(33) Finley, J.; Malmqvist, P.-Å.; Roos, B. O.; Serrano-Andrés, L. The Multi-State CASPT2 Method. *Chem. Phys. Lett.* **1998**, *288*, 299−306.
(34) Granovsky, A. A. Extended Multi-Configuration Quasi-Degenerate Perturbation Theory: The New Approach to Multi-State Multi-Reference Perturbation Theory. *J. Chem. Phys.* **2011**, *134*, 214113.
(35) Shiozaki, T.; Győrffy, W.; Celani, P.; Werner, H.-J. Communication: Extended Multi-State Complete Active Space Second-Order Perturbation Theory: Energy and Nuclear Gradients. *J. Chem. Phys.* **2011**, *135*, 081106.
(36) Nakano, H. Quasidegenerate Perturbation Theory with Multiconfigurational Self-Consistent-Field Reference Functions. *J. Chem. Phys.* **1993**, *99*, 7983−7992.
(37) Nakano, H. MCSCF Reference Quasidegenerate Perturbation Theory with Epstein-Nesbet Partitioning. *Chem. Phys. Lett.* **1993**, *207*, 372−378.
(38) Yanai, T.; Saitow, M.; Xiong, X.-G.; Chalupský, J.; Kurashige, Y.; Guo, S.; Sharma, S. Multistate Complete-Active-Space Second-Order Perturbation Theory Based on Density Matrix Renormalization Group Reference States. *J. Chem. Theory Comput.* **2017**, *13*, 4829−4840.
(39) Sommerfeld, T.; Ehara, M. Short-Range Stabilizing Potential for Computing Energies and Lifetimes of Temporary Anions with Extrapolation Methods. *J. Chem. Phys.* **2015**, *142*, 034105.
(40) Sommerfeld, T.; Ehara, M. Complex Absorbing Potentials with Voronoi Isosurfaces Wrapping Perfectly Around Molecules. *J. Chem. Theory Comput.* **2015**, *11*, 4627−4633.
(41) Ehara, M.; Fukuda, R.; Sommerfeld, T. Projected CAP/SAC-CI Method with Smooth Voronoi Potential for Calculating Resonance States. *J. Comput. Chem.* **2016**, *37*, 242−249.
(42) Sommerfeld, T.; Melugin, J. B.; Ehara, M. Temporary Anion States of Ethene Interacting with Single Molecules of Methane, Ethane, and Water. *J. Phys. Chem. A* **2018**, *122*, 2580−2586.
(43) Yanai, T.; Kurashige, Y.; Mizukami, W.; Chalupský, J.; Lan, T. N.; Saitow, M. Density Matrix Renormalization Group for Ab Initio Calculations and Associated Dynamic Correlation Methods: A Review of Theory and Applications. *Int. J. Quantum Chem.* **2015**, *115*, 283−299.
(44) Gamow, G. Zur Quantentheorie des Atomkernes. *Z. Phys.* **1928**, *51*, 204−212.
(45) Siegert, A. J. F. On the Derivation of the Dispersion Formula for Nuclear Reactions. *Phys. Rev.* **1939**, *56*, 750−752.
(46) Becke, A. D. Density-Functional Thermochemistry. III. The Role of Exact Exchange. *J. Chem. Phys.* **1993**, *98*, 5648−5652.
(47) Dunning, T. H., Jr. Gaussian Basis Sets for Use in Correlated Molecular Calculations. I. The Atoms Boron through Neon and Hydrogen. *J. Chem. Phys.* **1989**, *90*, 1007−1023.
(48) Ehara, M.; Kanazawa, Y.; Sommerfeld, T. Low-lying $\pi^*$ Resonances Associated with Cyano Groups: A CAP/SAC-CI Study. *Chem. Phys.* **2017**, *482*, 169−177.
(49) Angeli, C.; Borini, S.; Ferrighi, L.; Cimiraglia, R. Ab Initio N-Electron Valence State Perturbation Theory Study of the Adiabatic Transitions in Carbonyl Molecules: Formaldehyde, Acetaldehyde, and Acetone. *J. Chem. Phys.* **2005**, *122*, 114304.
(50) Nakatsuji, H. Cluster Expansion of the Wavefunction. Excited States. *Chem. Phys. Lett.* **1978**, *59*, 362−364.
(51) Nakatsuji, H. Cluster Expansion of the Wavefunction. Electron Correlations in Ground and Excited States by SAC (Symmetry-Adapted-Cluster) and SAC CI Theories. *Chem. Phys. Lett.* **1979**, *67*, 329−333.
(52) Fukuda, R.; Nakatsuji, H. Formulation and Implementation of Direct Algorithm for the Symmetry-Adapted Cluster and Symmetry-Adapted Cluster-Configuration Interaction Method. *J. Chem. Phys.* **2008**, *128*, 094105.
(53) Nakatsuji, H. Cluster Expansion of the Wavefunction, Valence and Rydberg Excitations, Ionizations, and Inner-Valence Ionizations of $CO_2$ and $N_2O$ Studied by the SAC and SAC CI Theories. *Chem. Phys.* **1983**, *75*, 425−441.
(54) Fukuda, R.; Ehara, M. Efficiency of Perturbation-Selection and Its Orbital Dependence in the SAC-CI Calculations for Valence Excitations of Medium-Size Molecules. *J. Comput. Chem.* **2014**, *35*, 2163−2176.
(55) Frisch, M. J.; Trucks, G. W.; Schlegel, H. B.; Scuseria, G. E.; Robb, M. A.; Cheeseman, J. R.; Scalmani, G.; Barone, V.; Mennucci, B.; Petersson, G. A. et al. *GAUSSIAN09* Rev. B.01; Gaussian Inc.: Wallingford CT, 2010.
(56) Woon, D. E.; Dunning, T. H., Jr. Gaussian Basis Sets for Use in Correlated Molecular Calculations. III. The Atoms Aluminum through Argon. *J. Chem. Phys.* **1993**, *98*, 1358−1371.
(57) Choi, Y.; Jordan, K. D. Electron Transmission Spectra of Carbonyl Fluoride: Determination of the Vertical Electron Affinity. *Chem. Phys. Lett.* **1989**, *156*, 450−454.
(58) Burrow, P. D.; Michejda, J. A. Electron Transmission Study of the Formaldehyde Electron Affinity. *Chem. Phys. Lett.* **1976**, *42*, 223−226.
(59) Benoit, C.; Abouaf, R. Low-Energy Electron Collisions with Formaldehyde: Interference Phenomena in the Differential Vibrational Excitation Cross Section. *Chem. Phys. Lett.* **1986**, *123*, 134−138.
(60) Schneider, B. I.; Rescigno, T. N.; McCurdy, C. W. Resonant Vibrational Excitation of $H_2CO$ by Low-Energy Electron Impact. *Phys. Rev. A: At., Mol., Opt. Phys.* **1990**, *42*, 3132−3134.
(61) Mahalakshmi, S.; Mishra, M. K. The $^2B_1$ Shape Resonance in Electron-Formaldehyde Scattering: An Investigation Using the Dilated Electron Propagator Method. *Chem. Phys. Lett.* **1998**, *296*, 43−50.
(62) Kaur, S.; Baluja, K. L. Electron-Impact Study of Formaldehyde Using the R-Matrix Method. *J. Phys. B: At., Mol. Opt. Phys.* **2005**, *38*, 3917−3933.
(63) Vinodkumar, M.; Bhutadia, H.; Antony, B.; Mason, N. Electron-Impact Rotationally Elastic Total Cross Sections for $H_2CO$ and HCOOH over a Wide Range of Incident Energy (0.01-2000 eV). *Phys. Rev. A: At., Mol., Opt. Phys.* **2011**, *84*, 052701.
(64) Gallup, G. A. Application of the Finite-Element-Discrete-Model Method for Calculating Resonance Properties. *Phys. Rev. A: At., Mol., Opt. Phys.* **2011**, *84*, 012701.
(65) Pal, S.; Vaval, N.; Sajeev, Y. Shape Resonance in Electron Molecule Scattering Using Coupled Cluster Method. *Indian J. Phys.* **2007**, *81*, 1061−1067.
(66) Feuerbacher, S.; Sommerfeld, T.; Cederbaum, L. S. Intersections of Potential Energy Surfaces of Short-Lived States: The Complex Analogue of Conical Intersections. *J. Chem. Phys.* **2004**, *120*, 3201−3214.
(67) Skalický, T.; Chollet, C.; Pasquier, N.; Allan, M. Properties of the Π* and Σ* States of the Chlorobenzene Anion Determined by Electron Impact Spectroscopy. *Phys. Chem. Chem. Phys.* **2002**, *4*, 3583−3590.
(68) Wiley, J. R.; Chen, E. C. M.; Wentworth, W. E. Bound Excited States of Chloroethylene Anions Studied by Electron Capture Negative Ion Mass Spectrometry. *J. Phys. Chem.* **1993**, *97*, 1256−1257.
(69) Modelli, A. Electron Attachment and Intramolecular Electron Transfer in Unsaturated Chloroderivatives. *Phys. Chem. Chem. Phys.* **2003**, *5*, 2923−2930.


https://dx.doi.org/10.1021/acs.jctc.9b01032
J. Chem. Theory Comput. 2020, 16, 2606−2616

(70) Modelli, A.; Venuti, M. Temporary Π* and Σ* Anions and Dissociative Electron Attachment in Chlorobenzene and Related Molecules. *J. Phys. Chem. A* **2001**, *105*, 5836−5841.
(71) Olthoff, J. K.; Tossell, J. A.; Moore, J. H. Electron Attachment by Haloalkenes and Halobenzenes. *J. Chem. Phys.* **1985**, *83*, 5627−5634.
(72) Stricklett, K. L.; Chu, S. C.; Burrow, P. D. Dissociative Attachment in Vinyl and Allyl Chloride, Chlorobenzene and Benzyl Chloride. *Chem. Phys. Lett.* **1986**, *131*, 279−284.
(73) Burrow, P. D.; Modelli, A.; Chiu, N. S.; Jordan, K. D. Temporary Σ and Π Anions of the Chloroethylenes and Chlorofluoroethylenes. *Chem. Phys. Lett.* **1981**, *82*, 270−276.
(74) Stockdale, J. A.; Hurst, G. S. Swarm Measurement of Cross Sections for Dissociative Electron Capture in Heavy Water, Chlorobenzene, and Bromobenzene. *J. Chem. Phys.* **1964**, *41*, 255−261.
(75) Kaufel, R.; Illenberger, E.; Baumgärtel, H. Formation and Dissociation of the Chloroethylene Anions. *Chem. Phys. Lett.* **1984**, *106*, 342−346.
(76) Sommerfeld, T. Electron-Induced Chemistry of 5-Chlorouracil. *ChemPhysChem* **2001**, *2*, 677−679.
(77) Aflatooni, K.; Burrow, P. D. Total Cross Sections for Dissociative Electron Attachment in Dichloroalkanes and Selected Polychloroalkanes: The Correlation with Vertical Attachment Energies. *J. Chem. Phys.* **2000**, *113*, 1455−1464.
(78) Benda, Z.; Jagau, T.-C. Understanding Processes Following Resonant Electron Attachment: Minimum-Energy Crossing Points between Anionic and Neutral Potential Energy Surfaces. *J. Chem. Theory Comput.* **2018**, *14*, 4216−4223.
(79) Gallup, G. A.; Burrow, P. D.; Fabrikant, I. I. Reply to "Comment on 'Electron-Induced Bond Breaking at Low Energies in HCOOH and Glycine: The Role of Very Short-Lived $\sigma^*$ Anion States'". *Phys. Rev. A: At., Mol., Opt. Phys.* **2009**, *80*, 046702.
(80) Schulz, G. J. Resonances in Electron-Impact on Diatomic-Molecules. *Rev. Mod. Phys.* **1973**, *45*, 423−486.
(81) Kennerly, R. E. Absolute Total Electron Scattering Cross Sections for $N_2$ Between 0.5 and 50 eV. *Phys. Rev. A: At., Mol., Opt. Phys.* **1980**, *21*, 1876−1883.
(82) Falcetta, M. F.; DiFalco, L. A.; Ackerman, D. S.; Barlow, J. C.; Jordan, K. D. Assessment of Various Electronic Structure Methods for Characterizing Temporary Anion States: Application to the Ground State Anions of $N_2$, $C_2H_2$, $C_2H_4$, and $C_6H_6$. *J. Phys. Chem. A* **2014**, *118*, 7489−7497.
(83) Izmaylov, A. F.; Adamson, S. O.; Zaitsevskii, A. Multi-partitioning Many-Body Perturbation Theory Calculations on Temporary Anions: Applications to $N_2^-$ and $CO^-$. *J. Phys. B: At., Mol. Opt. Phys.* **2004**, *37*, 2321−2329.
(84) Mahalakshmi, S.; Venkatnathan, A.; Mishra, M. K. Application of Higher Order Decouplings of the Dilated Electron Propagator to $^2\Pi$ $CO^-$, $^2\Pi_g$ $N_2^-$ and $^2\Pi_g$ $C_2H_2^-$ Shape Resonances. *J. Chem. Phys.* **2001**, *115*, 4549−4557.
(85) Honigmann, M.; Buenker, R. J.; Liebermann, H.-P. Complex Self-Consistent Field and Multireference Single- and Double-Excitation Configuration Interaction Calculations for the $^2\Pi_g$ Resonance State of $N_2^-$. *J. Chem. Phys.* **2006**, *125*, 234304.
(86) Sajeev, Y.; Santra, R.; Pal, S. Correlated Complex Independent Particle Potential for Calculating Electronic Resonances. *J. Chem. Phys.* **2005**, *123*, 204110.
(87) Sajeev, Y.; Santra, R.; Pal, S. Analytically Continued Fock Space Multireference Coupled-Cluster Theory: Application to the $^2\Pi_g$ Shape Resonance in e-$N_2$ Scattering. *J. Chem. Phys.* **2005**, *122*, 234320.
(88) Zhou, Y.; Ernzerhof, M. Calculating the Lifetimes of Metastable States with Complex Density Functional Theory. *J. Phys. Chem. Lett.* **2012**, *3*, 1916−1920.
(89) Gnaser, H. Formation of Metastable $N_2^-$ and $CO^-$ Anions in Sputtering. *Phys. Rev. A* **1997**, *56*, R2518.
(90) Middleton, R.; Klein, J. Production of Metastable Negative Ions in A Cesium Sputter Source: Verification of the Existence of $N_2^-$ and $CO^-$. *Phys. Rev. A* **1999**, *60*, 3786−3799.
(91) Sommerfeld, T.; Cederbaum, L. S. Long-Lived States of $N_2^-$. *Phys. Rev. Lett.* **1998**, *80*, 3723−3726.
(92) Andersen, T.; Bertelsen, K. A.; Raarup, M. K.; Rud, N.; Olsen, J.; Veseth, L. Long-Lived States of $N_2^-$: Formation, Lifetimes, and Identity. *Phys. Rev. A: At., Mol., Opt. Phys.* **1999**, *60*, 3627−3632.
(93) Lofthus, A.; Krupenie, P. H. The Spectrum of Molecular Nitrogen. *J. Phys. Chem. Ref. Data* **1977**, *6*, 113−307.
(94) Smith, D. W.; Day, O. W. Extension of Koopmans' Theorem. I. Derivation. *J. Chem. Phys.* **1975**, *62*, 113−114.


https://dx.doi.org/10.1021/acs.jctc.9b01032
*J. Chem. Theory Comput.* 2020, 16, 2606−2616